# Estimating the Subsonic Aerodynamic Center

# and Moment Components for Swept Wings

W. F. Phillips,[1] D. F. Hunsaker,[2]

*Utah State University, Logan, Utah 84322-4130*

and

R. J. Niewoehner[3]

*United States Naval Academy, Annapolis, Maryland 21402-5025*

**An improved method is presented for estimating the subsonic location of the semispan aerodynamic center of a swept wing and the aerodynamic moment components about that aerodynamic center. The method applies to wings with constant linear taper and constant quarter-chord sweep. The results of a computational fluid dynamics study for 236 wings show that the position of the semispan aerodynamic center of a wing depends primarily on aspect ratio, taper ratio, and quarter-chord sweep angle. Wing aspect ratio was varied from 4.0 to 20, taper ratios from 0.25 to 1.0 were investigated, quarter-chord sweep angles were varied from 0 to 50 degrees, and linear geometric washout was varied from −4.0 to +8.0 degrees. All wings had airfoil sections from the NACA 4-digit airfoil series with camber varied from 0 to 4 percent and thickness ranging from 6 to 18 percent. Within the range of parameters studied, wing camber, thickness, and twist were shown to have no significant effect on the position of the semispan aerodynamic center. The results of this study provide improved resolution of the semispan aerodynamic center and moment components for conceptual design and analysis.**

---

[1] Professor, Mechanical and Aerospace Engineering Department, 4130 Old Main Hill. Senior Member AIAA.

[2] Graduate Student, Mechanical and Aerospace Engineering Department, 4130 Old Main Hill. Student Member AIAA.

[3] Captain, US Navy, Aerospace Engineering Department, 590 Holloway Road. Member AIAA.

**Nomenclature**

$A_n$ = Fourier coefficients in the series solution to the lifting-line equation

$a_n$ = planform contribution to the Fourier coefficients in the series solution to the lifting-line equation

$b$ = wingspan

$b_n$ = twist contribution to the Fourier coefficients in the series solution to the lifting-line equation

$C_D$ = wing drag coefficient

$C_L$ = wing lift coefficient

$\widetilde{C}_L$ = total section lift coefficient

$\widetilde{C}_{L_a}$ = additional section lift coefficient

$\widetilde{C}_{L_b}$ = basic section lift coefficient

$C_{L,\alpha}$ = wing lift slope

$\widetilde{C}_{L,\alpha}$ = airfoil section lift slope

$(C_{\ell_0})_{\text{left}}$ = left wing semispan rolling moment coefficient about the origin, also equal to the root bending moment coefficient for the wing

$(C_{\ell_{ac}})_{\text{left}}$ = left wing semispan rolling moment coefficient about the aerodynamic center of left wing semispan

$(C_{\ell_{b0}})_{\text{left}}$ = basic lift contribution to left wing semispan rolling moment coefficient about the origin

$C_{m_0}$ = wing pitching moment coefficient about the origin

$C_{m_0,\alpha}$ = change wing pitching moment coefficient about the origin with respect to angle of attack

$C_{m_{ac}}$ = wing pitching moment coefficient about the aerodynamic center

$\widetilde{C}_{m_{ac}}$ = section pitching moment coefficient about the section aerodynamic center

$\overline{\widetilde{C}}_{m_{ac}}$ = mean section pitching moment coefficient about the section aerodynamic center, defined in Eq. (23)

$(C_{m_0})_{\text{left}}$ = left wing semispan pitching moment coefficient about the origin, also equal to the root twisting moment coefficient for the wing

$(C_{m_{ac}})_{\text{left}}$ = left wing semispan pitching moment coefficient about the aerodynamic center of left wing semispan

$c$ = local airfoil section chord length

$\bar{c}$ = geometric mean chord length, $S/b$

$\bar{c}_{mac}$ = mean aerodynamic chord length

$c_{\text{ref}}$ = reference chord length used to define the pitching moment coefficient

$c_{\text{root}}, c_{\text{tip}}$ = root and tip chord lengths

$\widetilde{L}$ = airfoil section lift

$R_A$ = wing aspect ratio, $b^2/S$

$R_T$ = wing taper ratio, $c_{\text{tip}}/c_{\text{root}}$

$S$ = wing planform area

$V_\infty$ = magnitude of the freestream velocity

$x$ = axial coordinate measured aft from the aerodynamic center of the centerline airfoil section

$x_{ac}$ = axial coordinate of the local wing section aerodynamic center

$\widetilde{x}_{ac}$ = axial coordinate of the local airfoil section aerodynamic center

$\bar{x}_{ac}$ = axial coordinate of the wing aerodynamic center

$\bar{x}_c$ = axial coordinate of the section aerodynamic center of the airfoil located at the centroidal chord, which

passes through the wing semispan area centroid

$y$ = normal coordinate measured upward from the aerodynamic center of the centerline airfoil section

$z$ = spanwise coordinate measured outboard from the wing centerline

$\bar{z}_{ac}$ = spanwise coordinate of the wing semispan aerodynamic center

$\bar{z}_c$ = spanwise coordinate of the centroidal chord, which passes through the wing semispan area centroid

$z_{mac}$ = spanwise coordinate of the wing mean aerodynamic chord

$\alpha$ = geometric angle of attack relative to the freestream

$\alpha_{L0}$ = airfoil section zero-lift angle of attack

$\Gamma$ = spanwise section circulation distribution

$\gamma_t$ = strength of shed vortex sheet per unit span

$\theta$ = change of variables for the spanwise coordinate, $\cos^{-1}(-2z/b)$

$\kappa_{ac}$ = sweep factor in the relation for wing aerodynamic center

$\kappa_{L\Lambda}$ = sweep factor in the relation for wing lift slope

$\kappa_{M\Lambda}$ = sweep factor in relation for wing pitching moment about the wing aerodynamic center

$\kappa_{M\Omega}$ = twist factor in relations for semispan moment components about the semispan aerodynamic center

$\Lambda$ = quarter-chord sweep angle

$\rho_\infty$ = freestream air density

$\Omega$ = maximum total twist, geometric plus aerodynamic

$\omega$ = normalized twist distribution function

## Introduction

The spanwise distribution of section aerodynamic loads acting on each semispan of a finite wing can be replaced with a resultant force vector acting at the aerodynamic center of the semispan and a resultant moment vector that does not vary with small changes in angle of attack. Because drag is typically small compared with the lift, drag is commonly neglected in estimating the position of the aerodynamic center and the resultant aerodynamic moment. See, for example, Etkin and Reid [1], McCormick [2], Pamadi [3], or Raymer [4].

When drag is neglected, the resultant aerodynamic moment produced on each semispan of a wing about the semispan aerodynamic center can be resolved into a pitching component about the span axis and a rolling component about the freestream velocity vector. The axial position of the wing semispan aerodynamic center is significant because it affects aircraft pitch stability and because the resultant aerodynamic force acting through this moment arm contributes to the structural twisting moment for a swept wing. The spanwise position of the semispan aerodynamic center is also important because knowledge of this location is useful in determining the wing bending moment. The semispan pitching moment about the semispan aerodynamic center is of interest because it affects aircraft trim and contributes to the wing twisting moment. Knowledge of the semispan rolling moment about the semispan aerodynamic center is valuable because this contributes directly to the wing bending moment. The spanwise location of the semispan aerodynamic center is also of use in the preliminary analysis of vertical stabilizers, where it is beneficial as a descriptor of the aircraft rolling moment contributed by such surfaces.

As a first approximation, the aerodynamic center of each wing semispan is sometimes assumed to be located at the section aerodynamic center of the airfoil section located at the spanwise coordinate of the semispan area centroid. Here the chord line that passes through the semispan area centroid is referred to as the *centroidal chord*. The spanwise coordinate of the wing semispan area centroid is given by [2,4],

$$\bar{z}_c \equiv \frac{2}{S} \int\limits_{z=0}^{b/2} cz\,dz \qquad (1)$$

For wings with constant linear taper, i.e., trapezoidal wings, Eq. (1) results in [1−4]

$$\frac{\bar{z}_c}{b} = \frac{1}{6}\frac{1+2R_T}{1+R_T} \qquad (2)$$

For wings of elliptic planform, the spanwise coordinate of the semispan centroid is given by [1]

$$\frac{\bar{z}_c}{b} = \frac{2}{3\pi} \cong 0.212 \qquad (3)$$

The location specified by Eq. (2) is commonly referred to as the location of the *mean aerodynamic chord* [4],

$$\bar{c}_{mac} \equiv \frac{2}{S} \int_{z=0}^{b/2} c^2 dz \qquad (4)$$

Referring to the centroidal chord of a trapezoidal wing as the mean aerodynamic chord can be misleading, because it could be taken to imply that the location of the mean aerodynamic chord is significant for other wing geometries as well. However, the mean aerodynamic chord passes through the semispan centroid only for the special case of a trapezoidal wing. For example, the mean aerodynamic chord of an elliptic wing is located at

$$\frac{z_{mac}}{b} = \frac{1}{6\pi}\sqrt{9\pi^2 - 64} \cong 0.264 \qquad (5)$$

whereas the centroidal chord is located according to Eq. (3).

*In general, the semispan aerodynamic center of a wing is not located along either the centroidal chord or the mean aerodynamic chord.* For example, Fig. 1 shows the aerodynamic center, centroidal chord, and mean aerodynamic chord for several different semispan geometries. As noted by Etkin and Reid [1] and McCormick [2], Eq. (1) gives the true spanwise location of the semispan aerodynamic center only if the additional section lift coefficient is uniform across the wingspan. Because a uniform additional section lift coefficient is produced by an elliptic wing with no sweep or dihedral in the locus of airfoil section aerodynamic centers, the semispan aerodynamic center of such wings is located along the centroidal chord as specified by Eq. (3). However, wings with linear taper do not produce a uniform additional section lift coefficient. Thus, Eq. (2) should be used only as a rough estimate for the semispan aerodynamic center of a trapezoidal wing.

To examine how the spanwise variation in wing section chord length affects the location of the semispan aerodynamic center, Prandtl's classical lifting-line theory [5,6] can be used to obtain an analytical solution for the spanwise variation in local section lift coefficient for a wing having no sweep or dihedral in the locus of airfoil section aerodynamic centers. For a wing of arbitrary planform and twist, this solution can be expressed in terms of a Fourier sine series
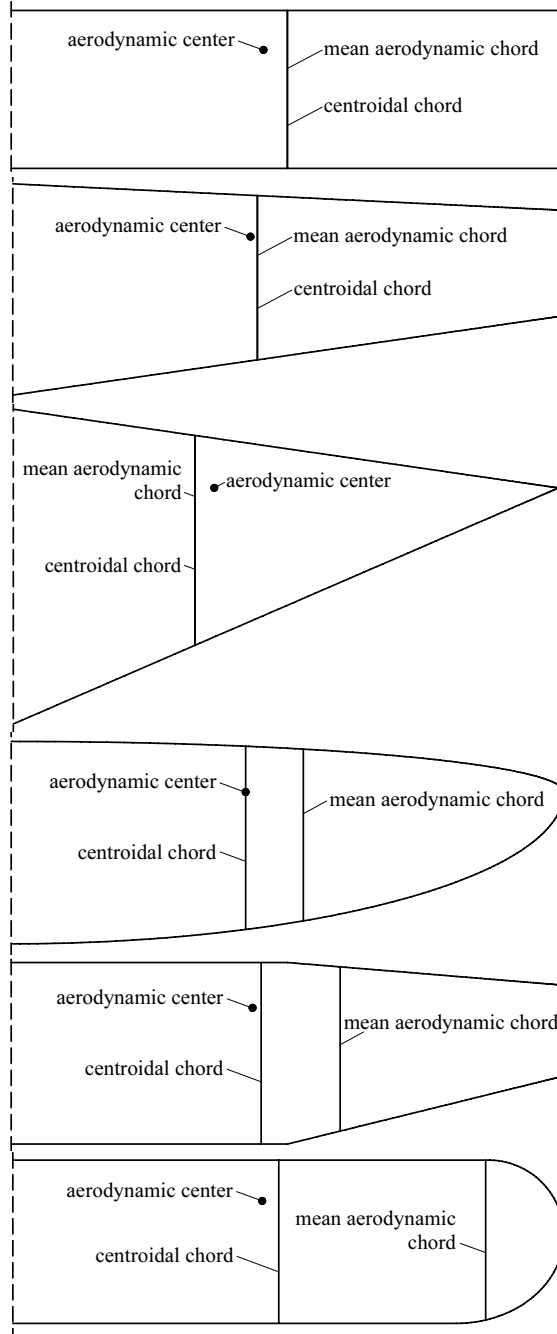
$$\widetilde{C}_L(\theta) \equiv \frac{\widetilde{L}(\theta)}{\frac{1}{2}\rho_\infty V_\infty^2 c(\theta)} = \frac{4b}{c(\theta)}\sum_{n=1}^{\infty} A_n \sin(n\theta) \qquad (6)$$

where

$$\theta \equiv \cos^{-1}(-2z/b) \qquad (7)$$

and the Fourier coefficients, $A_n$, must satisfy the relation

$$\sum_{n=1}^{\infty} A_n \left[ \frac{4b}{\widetilde{C}_{L,\alpha} c(\theta)} + \frac{n}{\sin(\theta)} \right] \sin(n\theta) = \alpha(\theta) - \alpha_{L0}(\theta) \quad (8)$$



**Fig. 1    Aerodynamic center, centroidal chord, and mean aerodynamic chord for six different semispan geometries, all having the same aspect ratio and no quarter-chord sweep.**

In Eq. (8) $\alpha$ and $\alpha_{L0}$ are allowed to vary with the spanwise coordinate to account for geometric and aerodynamic twist. Methods for evaluating the Fourier coefficients from Eq. (8) are varied and well known [7–10]. For a detailed presentation of Prandtl's lifting-line theory see Anderson [11], Bertin [12], Katz and Plotkin [13], Kuethe and Chow [14], McCormick [15], or Phillips [16].

## Analytical Solution for Unswept Wings

The section lift distribution specified by Eq. (6) can be used to obtain an analytical solution for the location of the semispan aerodynamic center of an unswept wing. Using an alternate form of the lifting-line solution for twisted wings [16–19], it has been shown that Eq. (6) can be written as [20]

$$\tilde{C}_L(\theta) = \Omega \sum_{n=1}^{\infty} 4\left(\frac{b_1 a_n}{a_1} - b_n\right) \frac{\sin(n\theta)}{c(\theta)/b} + C_L \sum_{n=1}^{\infty} \frac{4a_n}{\pi R_A a_1} \frac{\sin(n\theta)}{c(\theta)/b} \tag{9}$$

where $\Omega$ is defined to be the maximum total washout, geometric plus aerodynamic,

$$\Omega \equiv (\alpha - \alpha_{L0})_{\text{root}} - (\alpha - \alpha_{L0})_{\text{max}} \tag{10}$$

the Fourier coefficients, $a_n$ and $b_n$, are obtained from

$$\sum_{n=1}^{\infty} a_n \left[\frac{4b}{\tilde{C}_{L,\alpha} c(\theta)} + \frac{n}{\sin(\theta)}\right] \sin(n\theta) = 1 \tag{11}$$

$$\sum_{n=1}^{\infty} b_n \left[\frac{4b}{\tilde{C}_{L,\alpha} c(\theta)} + \frac{n}{\sin(\theta)}\right] \sin(n\theta) = \omega(\theta) \tag{12}$$

and $\omega(\theta)$ is the twist distribution normalized with respect to the maximum total washout

$$\omega(\theta) \equiv \frac{\alpha(\theta) - \alpha_{L0}(\theta) - (\alpha - \alpha_{L0})_{\text{root}}}{(\alpha - \alpha_{L0})_{\text{max}} - (\alpha - \alpha_{L0})_{\text{root}}} \tag{13}$$

The net wing lift coefficient for a twisted wing as obtained from this lifting-line solution is given by

$$C_L = \pi R_A [a_1(\alpha - \alpha_{L0})_{\text{root}} - b_1 \Omega] \tag{14}$$

For a detailed presentation of this solution to Prandtl's lifting-line equation, including several worked example problems, see Phillips [16].

We see from Eq. (9) that the spanwise variation in local section lift coefficient can be divided conveniently into two components. The first series on the right-hand side of Eq. (9) is called the *basic section lift coefficient* and the

second series is called the *additional section lift coefficient*. The basic section lift coefficient is independent of $C_L$ and directly proportional to the total amount of wing twist, $\Omega$. The additional section lift coefficient at any section of the wing is independent of wing twist and directly proportional to the net wing lift coefficient, $C_L$.

As can be seen from Eq. (9), *the basic section lift coefficient is the spanwise variation in local section lift coefficient that occurs when the total net lift developed by the wing is zero.* Examination of the first series on the right-hand side of Eq. (9) reveals that the basic section lift coefficient depends on all of the Fourier coefficients $a_n$ and $b_n$. From Eq. (11) we see the Fourier coefficients $a_n$ depend only on the wing planform. Equation (12) shows that the Fourier coefficients $b_n$ depend on both the wing planform and the dimensionless twist distribution function, $\omega(\theta)$. Thus, the spanwise variation in the basic section lift coefficient depends on wing planform and wing twist but is independent of the wing's angle of attack.

Examination of the second series on the right-hand side of Eq. (9) discloses that the additional section lift coefficient depends only on the wing planform and the Fourier coefficients $a_n$. From Eq. (11) we have seen that the $a_n$ coefficients do not depend on wing twist. Thus, Eq. (9) exposes the important fact that the additional section lift coefficient is independent of wing twist. Because the basic section lift coefficient is zero for an untwisted wing, we see that *the additional section lift coefficient is equivalent to the spanwise variation in local section lift coefficient that would be developed on an untwisted wing of the same planform operating at the same wing lift coefficient.*

Figure 2 shows how the net section lift coefficient and its two components from Eq. (9) vary along the span of a linearly tapered wing of aspect ratio 8.0 and taper ratio 0.5. This figure shows the spanwise variation in section lift coefficient for several values of total linear twist with the net wing lift coefficient held constant at 1.0. Similar results are shown in Fig. 3 for three different values of the net wing lift coefficient with the total linear twist held constant at 6 degrees. Notice that, whereas the center of total lift on each semispan moves inboard as washout is increased, the center of additional lift on each semispan does not change with either the amount of wing twist or the net wing lift coefficient. Here we will use the notation,

$$\widetilde{C}_{L_b}(\theta) \equiv \Omega \sum_{n=1}^{\infty} 4\left(\frac{b_1 a_n}{a_1} - b_n\right) \frac{\sin(n\theta)}{c(\theta)/b} \qquad (15)$$
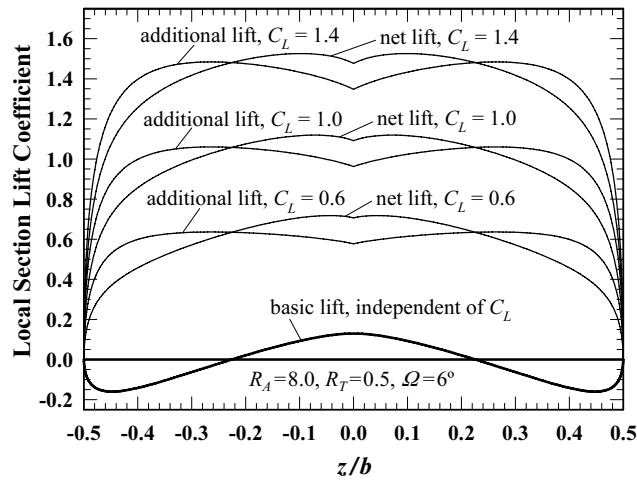
and

$$\widetilde{C}_{L_a}(\theta) \equiv C_L \sum_{n=1}^{\infty} \frac{4a_n}{\pi R_A a_1} \frac{\sin(n\theta)}{c(\theta)/b} \qquad (16)$$
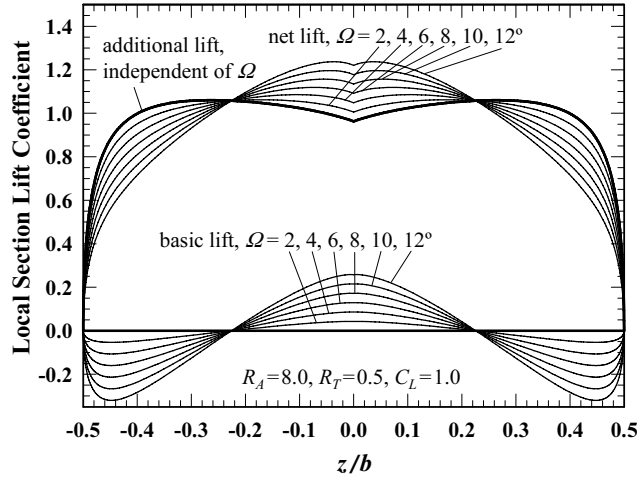
**Fig. 2  Spanwise variation in local section lift coefficient as a function of the total amount of linear twist with the net wing lift coefficient held constant at 1.0.**



**Fig. 3  Spanwise variation in local section lift coefficient as a function of the net wing lift coefficient with the total amount of linear twist held constant at 6º.**

Because we are neglecting drag, the resultant aerodynamic moment produced on each semispan of a wing about the origin of the coordinate system shown in Fig. 4 can be resolved into a pitching component about the *z*-axis and a rolling component about the freestream velocity vector.  The contribution of the left wing semispan to the rolling moment coefficient about the origin of the coordinate system shown in Fig. 4 is

$$(C_{\ell_0})_{\text{left}} = \frac{1}{Sb} \int_{z=0}^{b/2} (\widetilde{C}_{L_b} + \widetilde{C}_{L_a}) c \, z \, dz \qquad (17)$$
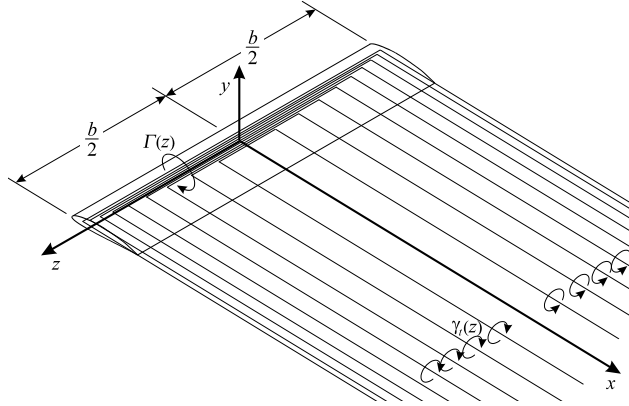
**Fig. 4   Prandtl's model for the vorticity generated by a wing of finite span.**

It is important to note that, within the small angle approximation, the moment coefficient specified by Eq. (17) is also the root bending moment coefficient resulting from the aerodynamic load on the wing.  Because section lift does not contribute to the pitching moment about the wing's lifting line, the contribution of the left semispan of an unswept wing to the pitching moment coefficient about the origin of the coordinate system shown in Fig. 4 is

$$(C_{m_0})_{\text{left}} = \frac{1}{S c_{\text{ref}}} \int_{z=0}^{b/2} \widetilde{C}_{m_{ac}} c^2 \, dz \qquad (18)$$

The moment coefficient specified by Eq. (18) can also be thought of as the root twisting moment coefficient resulting from the aerodynamic load on this unswept wing.

Equating the distributed section loads to resultant force and moment vectors acting at the aerodynamic center of the wing semispan, Eqs. (17) and (18) yield

$$
\begin{aligned}
(C_{\ell_{ac}})_{\text{left}} &+ \frac{\overline{z}_{ac}}{Sb} \int_{z=0}^{b/2} (\widetilde{C}_{L_b} + \widetilde{C}_{L_a}) c \, dz \\
&= \frac{1}{Sb} \int_{z=0}^{b/2} (\widetilde{C}_{L_b} + \widetilde{C}_{L_a}) c \, z \, dz
\end{aligned}
\qquad (19)
$$

$$(C_{m_{ac}})_{\text{left}} = \frac{1}{S c_{\text{ref}}} \int_{z=0}^{b/2} \widetilde{C}_{m_{ac}} c^2 \, dz \qquad (20)$$

The term on the right-hand side of Eq. (20) results from the effects of wing camber and is independent of geometric twist.  For a wing with constant section pitching moment coefficient, Eq. (20) simply becomes

$$(C_{m_{ac}})_{\text{left}} = \frac{\overline{c}_{mac}}{c_{\text{ref}}} \frac{\widetilde{C}_{m_{ac}}}{2} \qquad (21)$$

In a more general sense, Eq. (20) could be thought of in terms of a mean section pitching moment coefficient,

$$(C_{m_{ac}})_{\text{left}} = \frac{\overline{c}_{mac}}{c_{\text{ref}}} \frac{\overline{\widetilde{C}}_{m_{ac}}}{2} \tag{22}$$

where

$$\overline{\widetilde{C}}_{m_{ac}} \equiv \frac{2}{S\,\overline{c}_{mac}} \int\limits_{z=0}^{b/2} \widetilde{C}_{m_{ac}} c^2 dz \tag{23}$$

Because the resultant moment about the aerodynamic center is invariant to small changes in angle of attack, differentiating Eq. (19) with respect to angle of attack, applying Eqs. (15) and (16), and solving for $\overline{z}_{ac}/b$ gives

$$
\begin{aligned}
\frac{\overline{z}_{ac}}{b} &= \frac{2}{SbC_{L,\alpha}} \frac{\partial}{\partial\alpha} \int\limits_{z=0}^{b/2} (\widetilde{C}_{L_b} + \widetilde{C}_{L_a}) c\,z\,dz \\
&= \frac{2}{SbC_{L,\alpha}} \frac{\partial}{\partial\alpha} \int\limits_{z=0}^{b/2} \widetilde{C}_{L_a} c\,z\,dz \\
&= \frac{-2}{\pi} \sum_{n=1}^{\infty} \frac{a_n}{a_1} \int\limits_{\theta=\pi/2}^{\pi} \sin(n\theta)\cos\theta\,\sin\theta\,d\theta \\
&= \frac{1}{\pi} \sum_{n=1}^{\infty} \frac{a_n}{a_1} \int\limits_{\theta=\pi}^{\pi/2} \sin(n\theta)\sin(2\theta)\,d\theta
\end{aligned}
\tag{24}
$$

Because the additional section lift coefficient is independent of wing twist, Eq. (24) discloses the important fact that the spanwise position of the aerodynamic center of each wing semispan is not affected by wing twist. Recognizing that the even terms in $a_n$ are always zero for spanwise symmetric wings, the integration in Eq. (24) yields

$$
\begin{aligned}
\frac{\overline{z}_{ac}}{b} &= \frac{2}{3\pi} + \frac{2}{\pi} \sum_{n=3}^{\infty} \frac{\sin[(n-2)\pi/2]}{n^2-4} \frac{a_n}{a_1} \\
&= \frac{2}{3\pi} \left( 1 + \sum_{n=1}^{\infty} \frac{(-1)^{n-1}3}{4n^2+4n-3} \frac{a_{2n+1}}{a_1} \right)
\end{aligned}
\tag{25}
$$

Figure 5 shows how $\overline{z}_{ac}/b$ varies with taper ratio and aspect ratio for wings with constant linear taper. Notice that the location of the semispan aerodynamic center deviates significantly from the semispan area centroid, except for the special case of trapezoidal wings with a taper ratio near 0.35.

It can be shown from Eq. (24) that the spanwise coordinate of the semispan aerodynamic center can also be expressed as [1],

$$\overline{z}_{ac} = \frac{2}{SC_L} \int\limits_{z=0}^{b/2} \widetilde{C}_{L_a} c\,z\,dz \tag{26}$$
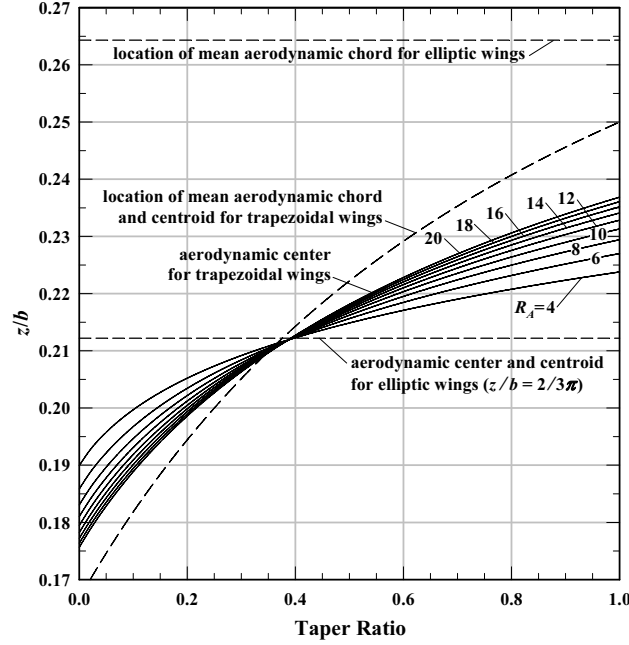
**Fig. 5   Aerodynamic center of wing semispan for unswept trapezoidal and elliptic wings.**

Using Eq. (26) in Eq. (17) yields

$$(C_{\ell_0})_{\text{left}} = \frac{\bar{z}_{ac} C_L}{2b} + \frac{1}{Sb} \int_{z=0}^{b/2} \widetilde{C}_{L_b} \, c \, z \, dz \qquad (27)$$

For wings with no sweep or dihedral, the integral on the right-hand side of Eq. (27) can be evaluated from Eq. (15). Following a development similar to that of Eq. (25) it is readily shown that, for spanwise symmetric wings with spanwise symmetric twist, using Eq. (15) in Eq. (27) produces

$$(C_{\ell_0})_{\text{left}} = \frac{\bar{z}_{ac} C_L}{2b} - \kappa_{M\Omega} \frac{C_{L,\alpha} \, \Omega}{2} \qquad (28)$$

where

$$\kappa_{M\Omega} \equiv \frac{2}{\pi} \frac{b_1}{a_1} \sum_{n=3}^{\infty} \frac{\sin[(n-2)\pi/2]}{n^2 - 4} \left( \frac{b_n}{b_1} - \frac{a_n}{a_1} \right)$$
$$= \frac{2}{\pi} \frac{b_1}{a_1} \sum_{n=1}^{\infty} \frac{(-1)^{n-1}}{4n^2 + 4n - 3} \left( \frac{b_{2n+1}}{b_1} - \frac{a_{2n+1}}{a_1} \right) \qquad (29)$$

It may be worth noting that the infinite series defined in Eq. (29) is dominated by the first term. For example, in the case of a rectangular wing of aspect ratio 6.0, carrying only the first term on the right-hand side of Eq. (29) yields $\kappa_{M\Omega} = 0.024340$, whereas carrying a very large number of terms in this infinite series produces $\kappa_{M\Omega} = 0.024989$.

For typical washout distributions $\kappa_{M\Omega}$ is positive. Figure 6 shows how $\kappa_{M\Omega}$ varies with taper ratio and aspect ratio for wings with constant linear taper and constant linear twist.

As expressed in Eq. (28), the root wing bending moment coefficient is composed of two components. The first is proportional to the semispan lift acting through a moment arm of $\bar{z}_{ac}$ and the second is proportional to the product of the wing lift slope and the wing twist. For a given wing planform, the value of the proportionality constant $\kappa_{M\Omega}$ depends on the way in which the twist is distributed along the wingspan. This dependence enters into Eq. (29) through the Fourier coefficients $b_n$, which depend on the twist distribution through Eq. (12). For the typical case where washout is greatest near the wingtips, $\kappa_{M\Omega}$ is positive as shown for the case of linear washout in Fig. 6. Thus, as might be expected, Eq. (28) shows that the root bending moment decreases linearly as washout is added at the wingtips. If a twist distribution were used that had the greatest washout near the wing root, then $\kappa_{M\Omega}$ would be negative and the root bending moment would increase in proportion to the amount of twist. For a given planform and twist distribution, Eq. (28) shows that the change in bending moment with respect to $\Omega$ is directly proportional to the wing lift slope. This should be expected because $C_{L,\alpha}$ is a measure of the wing's lift response to a change in any aerodynamic angle, i.e., $\alpha$, $\alpha_{L0}$, or $\Omega$. As shown by Phillips [17], the lift slope for a wing of arbitrary planform is not affected by wing twist.
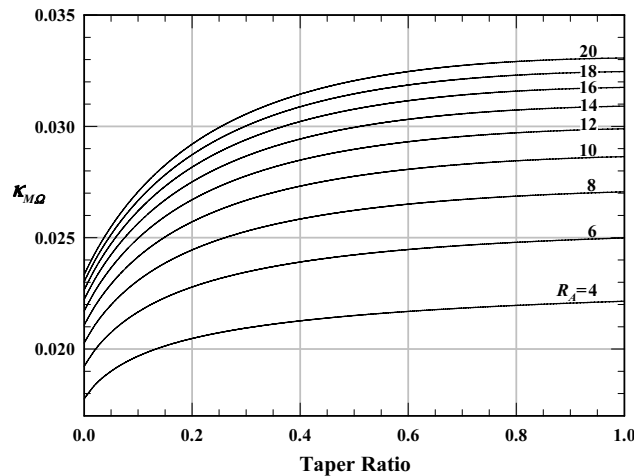


**Fig. 6  Twist factor in relations for semispan moment components about the semispan aerodynamic center.**

## Effects of Wing Sweep on Aerodynamic Center

The lifting-line result given by Eq. (25) does not apply directly to swept wings. Wing sweep affects the position of the semispan aerodynamic center in two ways. First and most obvious, when the wing is swept back, the locus of airfoil section aerodynamic centers on the outboard sections of the wing are moved aft of the aerodynamic center of the root airfoil section. Thus, lift developed on a swept wing contributes significantly to the pitching moment about the root airfoil section aerodynamic center [1]

$$
\begin{aligned}
C_{m_0} \;=\; & \frac{2}{S c_{\text{ref}}} \int_{z=0}^{b/2} \widetilde{C}_{m_{ac}} c^2 \, dz \\
& - \frac{2}{S c_{\text{ref}}} \int_{z=0}^{b/2} \widetilde{C}_L \, c \, x_{ac} \, dz
\end{aligned}
\tag{30}
$$

In addition, sweep alters the vorticity induced downwash distribution over the wing planform. Moving the wingtip vortex aft of the wing root tends to reduce the downwash induced on the inboard sections of the wing. On the other hand, the bound vorticity on one semispan of a swept wing induces downwash on the opposite semispan. This tends to increase the wing downwash, more so on the inboard sections of the wing. Thus, not only does sweep alter the geometry of the locus of airfoil section aerodynamic centers, it changes the spanwise section lift distribution as well.

The earliest methods used to estimate the aerodynamic center of a swept wing [21,22] ignored the change in lift distribution resulting from the sweep. Later experimental studies [23−26] showed that the aerodynamic center of a highly swept wing is shifted significantly as a result of the altered downwash. Not only does the spanwise section lift distribution vary with wing sweep, but the locus of wing section aerodynamic centers becomes shifted relative to the local airfoil section aerodynamic center. This shift is toward the trailing edge in the vicinity of the wing root and toward the leading edge near the wingtip, as shown in Fig. 7. The circular symbols on each wing semispan in this figure represent experimental data [23−26], the dashed line designates the locus of airfoil section aerodynamic centers, and the solid line is the locus of wing section aerodynamic centers predicted from the tangent approximation of Kuchemann [27]. Because the Fourier series solution to Prandtl's lifting-line equation does not apply to swept wings, predictions for the aerodynamic center of swept wings require numerical solutions. Panel codes and computational fluid dynamics (CFD) are commonly used for this purpose.

As a first approximation, the axial position of the aerodynamic center of a swept wing is sometimes assumed to be located at the section aerodynamic center of the airfoil section located at the spanwise coordinate of the semispan

area centroid [2,4]. For wings with constant quarter-chord sweep and constant linear taper, i.e., trapezoidal wings, Eq. (2) results in [1−4]

$$\frac{\overline{x}_{ac}}{\overline{c}} \cong \frac{\overline{x}_c}{\overline{c}} = \frac{R_A}{6}\frac{1+2R_T}{1+R_T}\tan\Lambda \qquad (31)$$

The approximation of Anderson [22] neglects any change in the lift distribution resulting from wing sweep, which from Eq. (25) yields

$$\frac{\overline{x}_{ac}}{\overline{c}} \cong \frac{2R_A}{3\pi}\left(1+\sum_{n=1}^{\infty}\frac{(-1)^{n-1}3}{4n^2+4n-3}\frac{a_{2n+1}}{a_1}\right)\tan\Lambda \qquad (32)$$

In the present paper, results obtained from a comprehensive CFD study are compared with the approximations given by Eqs. (31) and (32).
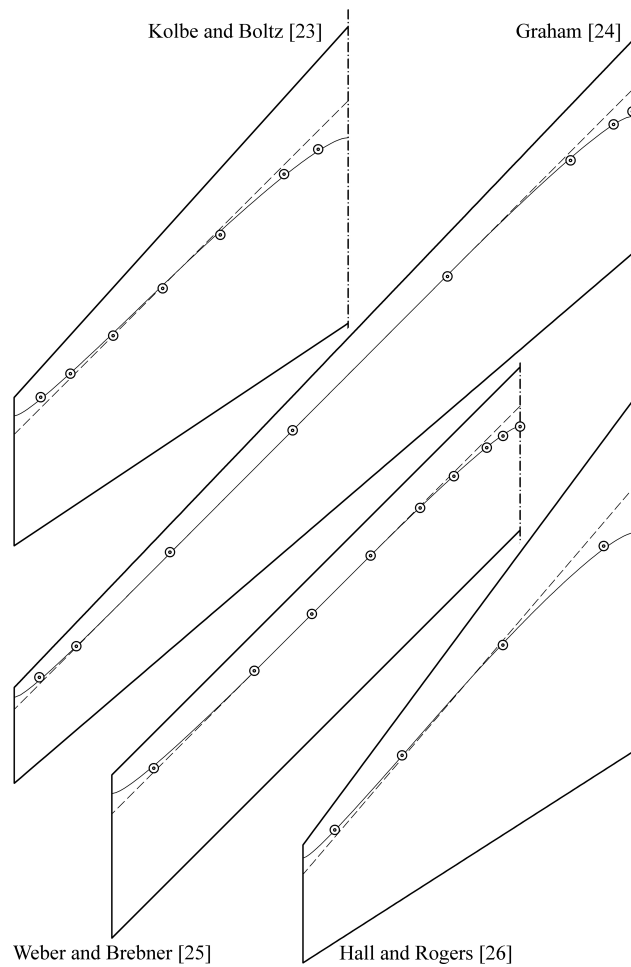


**Fig. 7   Shift in the locus of wing section aerodynamic centers due to wing sweep.**

## Computational Methodology

The distributed aerodynamic loads acting on the wing surface can be replaced with resultant force and moment vectors acting at the aerodynamic center of the wing. Thus, assuming that the aerodynamic center lies in the plane of the wing, the wing pitching moment coefficient about the origin can be written as

$$C_{m_0} = C_{m_{ac}} - (C_L \cos\alpha + C_D \sin\alpha)\bar{x}_{ac}/c_{\text{ref}} \qquad (33)$$

Neglecting the effects of drag and assuming small angles of attack, Eq. (33) is commonly approximated as [1−4]

$$C_{m_0} = C_{m_{ac}} - C_L\,\bar{x}_{ac}/c_{\text{ref}} \qquad (34)$$

Because the pitching moment about the aerodynamic center is invariant to small changes in angle of attack, the axial position of the wing aerodynamic center can be evaluated by differentiating Eq. (34) with respect to angle of attack and solving for $\bar{x}_{ac}/c_{\text{ref}}$. This gives

$$\frac{\bar{x}_{ac}}{c_{\text{ref}}} = -\frac{C_{m_0,\alpha}}{C_{L,\alpha}} \qquad (35)$$

The aerodynamic derivatives on the right-hand side of Eq. (35) could be obtained from either experimental data or computational methods. For the results presented here, CFD solutions were used.

All calculations were performed using version 6 of CFL3D [28]. In its most general form, CFL3D is a structured-grid, multi-zone code that solves the three-dimensional, time-dependent, Reynolds-averaged Navier-Stokes equations using an upwind finite-volume formulation. However, for the calculations presented herein, a steady inviscid formulation was employed, because only lift and pitching moment results are required to evaluate the position of the aerodynamic center from Eq. (35). The code uses a third-order upwind biased interpolation scheme for the convective and pressure terms, and the flux-difference-splitting method of Roe [29] is used to obtain the inviscid fluxes at cell faces. Local time stepping, mesh sequencing, and low-Mach-number preconditioning were also used. All results were obtained using a freestream Mach number of 0.10.

All computations were performed using C-O grids generated about one semispan of a finite wing. Inflow-outflow boundary conditions were specified on the far-field planes and symmetry conditions were used along the bounding plane at the wing root. Slip conditions were specified on the wing surface. Nodes were clustered in the normal direction near the wing surface and in the spanwise direction near the wingtip. Nodes were also clustered in the wake region aft of the wingtip, to provide improved resolution of the wingtip vortex. To keep the wingtip vortex confined to the wake region where nodes were clustered, a different grid was generated for each angle of attack

studied.  As the angle of attack was changed, the wing was rotated relative to the grid so that the freestream velocity vector was closely aligned with the *x*-axis of the grid and the region of wake clustering.  All wings had rounded end caps similar to that show in Fig. 8.  To aid in visibility, only the odd nodes in all three directions are shown in this figure.  For a more detailed description of the grids and grid generation software used for the present study see Phillips, Fugal, and Spall [19].
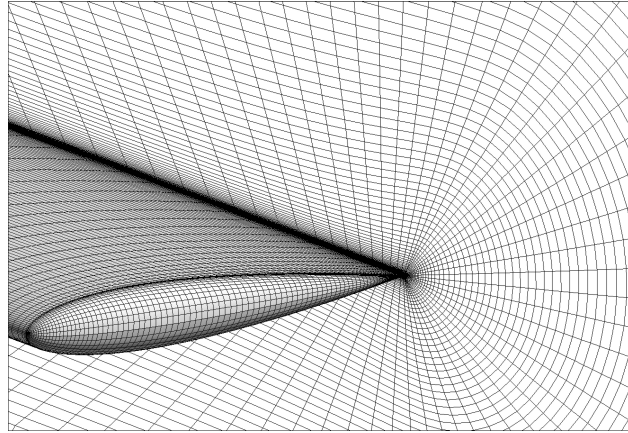


**Fig. 8   Constant-*j* planes at the trailing edge of the wing tip and constant-*k* plane on the wing surface.**

To ensure that the solutions were grid resolved for each wing and operating condition considered, mesh sequencing was employed in the solution procedure using coarse, intermediate, and fine grids, which contained 189,875, 1,473,333, and 11,606,441 nodes, respectively.  The fine grids had 121 spanwise sections with 289 nodes spaced around the circumference of each wing section.  An additional 208 streamwise nodes were included in the trailing wake for each spanwise section.  A total of 193 radial layers were used to create these 121×497×193 C-O grids.  The intermediate grids were obtained within CFL3D from the fine grids by deleting alternate points in each direction.  The coarse grids were derived from the intermediate grids in a similar manner.  Using converged results from the coarse, intermediate, and fine grids, an improved estimate for the grid resolved solution was obtained using the Richardson extrapolation [30,31].  To implement the extrapolation, the procedure described by Phillips, Fugal, and Spall [19] was used.

The nodes were distributed over a computational domain that extended 10 chord lengths from the wing in all directions.  For a subset of the calculations, a larger computational domain extending 20 chord lengths from the

wing in all directions was also used.  No significant changes in the solutions were observed for a computational domain greater than 10 chord lengths.

For each wing considered, the lift coefficient and the pitching moment coefficient about the aerodynamic center of the root airfoil section were determined from converged solutions for the coarse, intermediate, and fine grids, at angles of attack of −5.0, 0.0, and +5.0 degrees.  From these results, the Richardson extrapolations for the lift and pitching moment coefficients were obtained for these same angles of attack.  The position of the aerodynamic center was then evaluated from Eq. (35) for all three solutions and the Richardson extrapolation.  For each wing considered, grid convergence was assessed by comparing solutions obtained from the coarse, intermediate, and fine grids with that obtained from the Richardson extrapolation.  Typical results for these grid convergence studies are shown in Fig. 9.
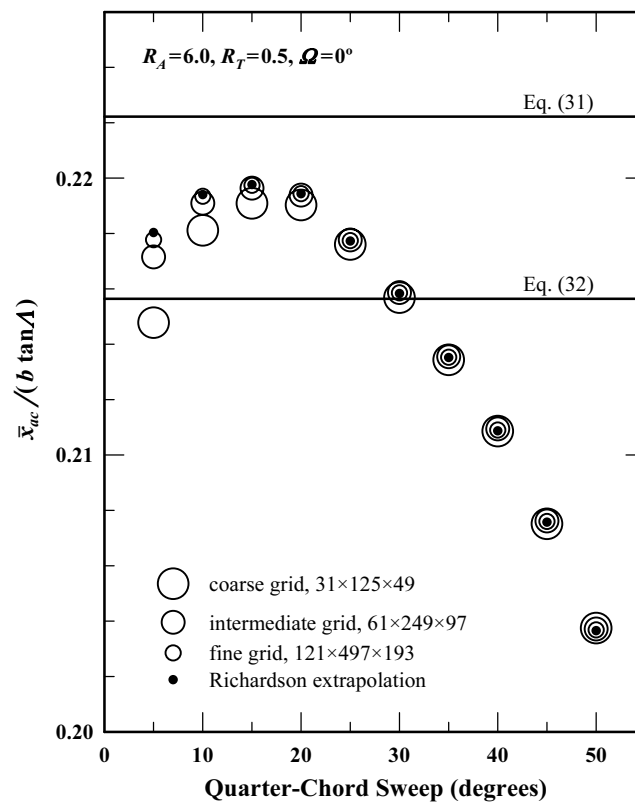


**Fig. 9   Grid-convergence study for untwisted swept wings of aspect ratio 6.0 and taper ratio 0.5.**

## CFD Results for Aerodynamic Center

A total of 236 wings with constant linear taper and constant quarter-chord sweep were considered in the present study. Wing aspect ratio was varied from 4.0 to 20 and taper ratios from 0.25 to 1.0 were investigated. For a given taper and aspect ratio, the quarter-chord sweep angle was varied from 0 to 50 degrees. All wings had airfoil sections from the NACA 4-digit airfoil series with camber varied from 0 to 4 percent and thickness ranging from 6 to 18 percent. To investigate the effects of wing twist, linear geometric washout was varied from −4.0 to +8.0 degrees.

Figure 10 shows how the aerodynamic center predictions evaluated from the CFD results obtained in the present study compare with results predicted from Eqs. (31) and (32). In this figure, the location of each aerodynamic center is presented as a deviation from the result predicted by Eq. (31). This deviation is plotted as a function of the same deviation as predicted from Eq. (32). To see how the data plotted in Fig. 10 are used to assess the accuracy of Eqs. (31) and (32), we first recognize that, if Eq. (31) were precise, each aerodynamic center would have the same axial coordinate as the airfoil section aerodynamic center of the semispan centroidal chord. Thus, exact correlation of Eq. (31) with the CFD results would cause all points in Fig. 10 to fall along a horizontal line with the vertical ordinate of zero. This is the line denoted as the Eq. (31) correlation line in Fig. 10. On the other hand, if Eq. (32)
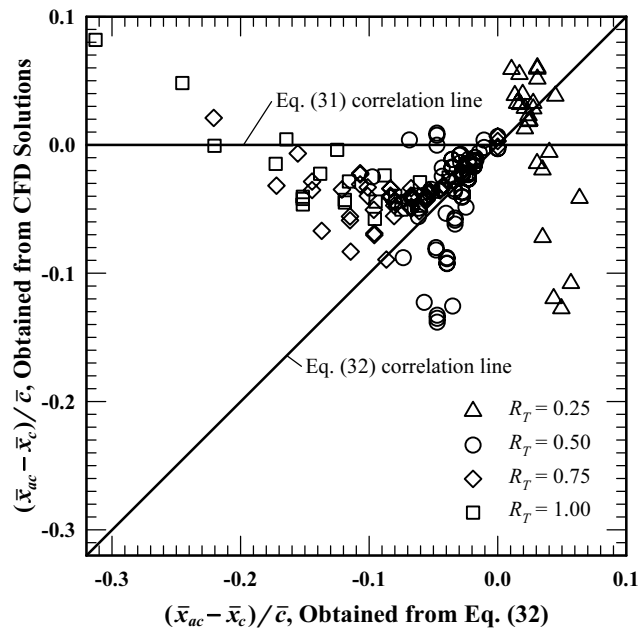


**Fig. 10   Deviation of wing aerodynamic center from the section aerodynamic center of the airfoil located at the semispan centroidal chord as predicted from CFD results vs. the same deviation predicted from Eq. (32).**

were to match the CFD predictions exactly, all points in Fig. 10 would fall along the 45-degree line, which is labeled as the Eq. (32) correlation line. From the results plotted in Fig. 10, we see that neither Eq. (31) nor Eq. (32) is accurate over a wide range of wing geometry. Notice that Eq. (31) seems to be more accurate for most of the rectangular wings, whereas the results for many of the wings having a taper ratio of 0.5 agree more closely with Eq. (32). The reader should particularly notice the heavy concentration of circular symbols just below the intersection of the Eq. (31) and Eq. (32) correlation lines. Most of these data are for wings having a taper ratio of 0.5 with quarter-chord sweep angles between 25 and 35 degrees. These results agree closely with Eq. (32) and show that, for such commonly used wing geometries, the lifting-line result presented in Eq. (32) gives a reasonable first approximation for the position of the aerodynamic center of the wing.

For swept trapezoidal wings, the results of the present CFD study can be used to improve the approximate theoretical-based result given by Eq. (32). Multiplying the right-hand side of Eq. (32) by an empirical sweep correction factor we obtain

$$\frac{\overline{x}_{ac}}{\overline{c}} \cong \kappa_{ac} \frac{2R_A}{3\pi} \left(1 + \sum_{n=1}^{\infty} \frac{(-1)^{n-1} 3}{4n^2 + 4n - 3} \frac{a_{2n+1}}{a_1}\right) \tan \Lambda \quad (36)$$

By correlating CFD results obtained in the present study, the empirical sweep correction factor shown in Fig. 11 was obtained as a function of wing taper ratio, aspect ratio, and quarter-chord sweep angle. This figure was obtained by correlating only the results for untwisted wings having the NACA 0012 airfoil section. Other results obtained in the present study show that wing camber, thickness, and twist have no significant effect on the position of the aerodynamic center of a wing.

In Fig. 11 note that, for wings of taper ratio near 0.5, aspect ratios in the range of 6 to 8, and quarter-chord sweep angles near 30 degrees, all values of $\kappa_{ac}$ are close to unity. This means that the lifting-line result presented in Eq. (32) provides a good approximation for this commonly used wing geometry, without using the empirical correction factor. On the other hand, both Fig. 10 and Fig. 11 show that some wing geometries result in very large discrepancies between Eq. (32) and the CFD results. These discrepancies are very significant because they can result in shifts in the neutral point that change the static margin by more than 5 percent, which is the same order of magnitude as the design static margin for typical aircraft.

Figure 12 shows all of the aerodynamic center predictions evaluated from the CFD results obtained in the present study compared with results predicted from Eq. (36) using the values for $\kappa_{ac}$ that are plotted in Fig. 11.

Figure 12 includes results obtained for twisted wings and wings with other airfoil sections, as well as the results used to obtain Fig. 11. Comparing Fig. 12 with Fig. 10, we see that using the empirical sweep correction factor plotted in Fig. 11 provides a very significant improvement over the uncorrected results of Eq. (32).
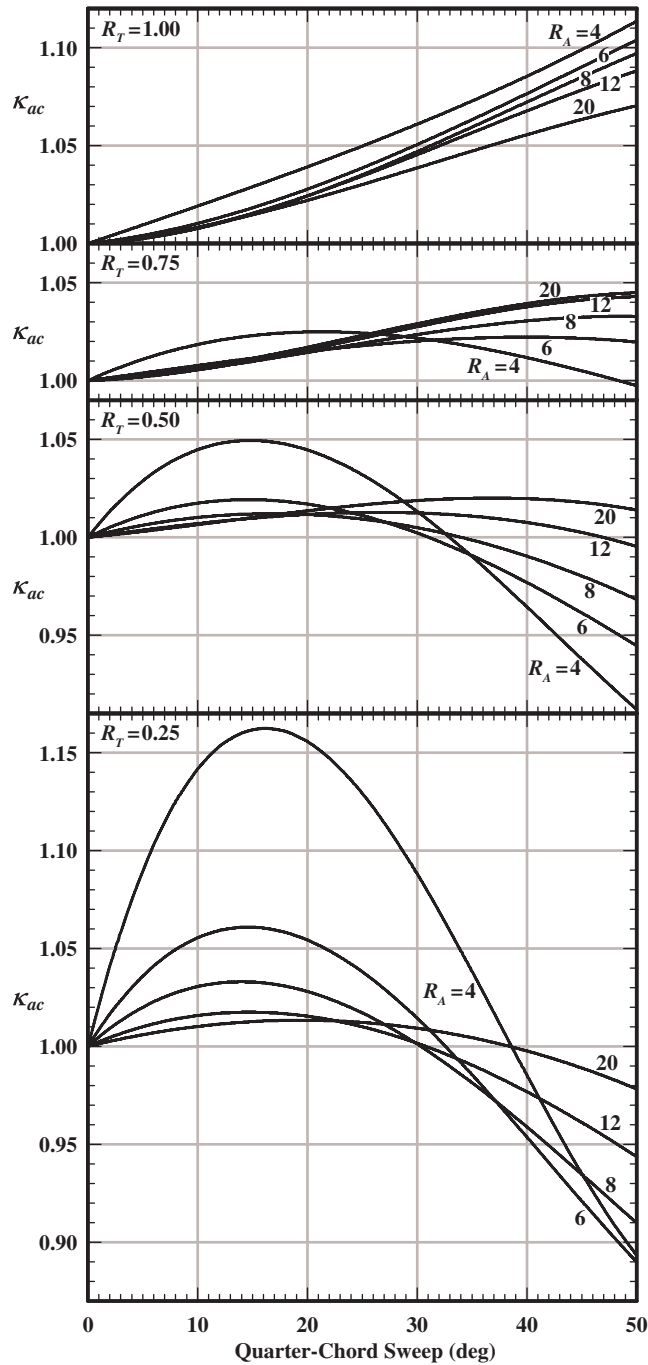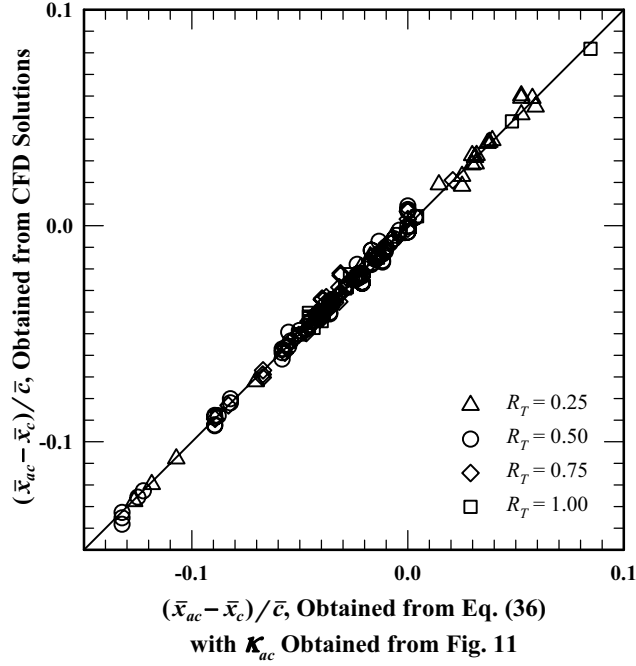


**Fig. 11   Effects of wing sweep on the location of the aerodynamic center of a wing.**

**Fig. 12   Deviation of wing aerodynamic center from the section aerodynamic center of the airfoil located at the semispan centroidal chord as predicted from CFD results vs. the same deviation predicted from Eq. (36).**

## Pitching Moment about the Aerodynamic Center

Once the location of the aerodynamic center is known, the pitching moment coefficient about the aerodynamic center can be determined from the lift coefficient and pitching moment coefficient about the origin.  Rearranging Eq. (34) yields

$$C_{m_{ac}} \;=\; C_{m_0} + C_L\, \bar{x}_{ac}/c_{\text{ref}} \tag{37}$$

and for a wing with constant quarter-chord sweep this gives

$$C_{m_{ac}} \;=\; C_{m_0} + \frac{\bar{z}_{ac}}{c_{\text{ref}}} C_L \tan\Lambda \tag{38}$$

The pitching moment coefficient about the origin is evaluated from Eq. (30).  Assuming that the locus of wing section aerodynamic centers follows the locus of airfoil section aerodynamic centers, this becomes

$$
\begin{aligned}
C_{m_0} \;=\;& \frac{2}{Sc_{\text{ref}}} \int_{z=0}^{b/2} \widetilde{C}_{m_{ac}}\, c^2\, dz \\
& - \frac{2}{Sc_{\text{ref}}} \int_{z=0}^{b/2} \widetilde{C}_L\, c\, \widetilde{x}_{ac}\, dz
\end{aligned}
\tag{39}
$$

which for a wing with constant quarter-chord sweep can be written as

$$
\begin{aligned}
C_{m_0} \;=\; & \frac{2}{S c_{\text{ref}}} \int_{z=0}^{b/2} \widetilde{C}_{m_{ac}} c^2 \, dz \\
& - \frac{2}{S c_{\text{ref}}} \int_{z=0}^{b/2} \widetilde{C}_L \, c \, z \, dz \, \tan \Lambda
\end{aligned}
\tag{40}
$$

Using Eq. (40) in Eq. (38) we obtain

$$
\begin{aligned}
C_{m_{ac}} \;=\; & \frac{2}{S c_{\text{ref}}} \int_{z=0}^{b/2} \widetilde{C}_{m_{ac}} c^2 \, dz \\
& - \frac{\tan \Lambda}{c_{\text{ref}}} \left( \frac{2}{S} \int_{z=0}^{b/2} \widetilde{C}_L \, c \, z \, dz - \bar{z}_{ac} C_L \right)
\end{aligned}
\tag{41}
$$

The total section lift coefficient is the sum of the basic and additional section lift coefficients, $\widetilde{C}_L = \widetilde{C}_{L_b} + \widetilde{C}_{L_a}$, and the spanwise coordinate of the semispan aerodynamic center can be expressed in terms of the additional section lift coefficient according to Eq. (26). Thus, the pitching moment coefficient about the aerodynamic center of the wing can be expressed in terms of only the airfoil section pitching moment coefficient and the spanwise variation in local section lift coefficient that occurs when the net lift developed by the wing is zero. Using Eq. (26) in Eq. (41) gives

$$
C_{m_{ac}} \;=\; \frac{2}{S c_{\text{ref}}} \int_{z=0}^{b/2} \widetilde{C}_{m_{ac}} c^2 \, dz - \frac{2 \tan \Lambda}{S c_{\text{ref}}} \int_{z=0}^{b/2} \widetilde{C}_{L_b} \, c \, z \, dz
\tag{42}
$$

The first term on the right-hand side of Eq. (42) results from the effects of camber and is simply twice the semispan contribution for an unswept wing, which is given by Eq. (20). The second term on the right-hand side of Eq. (42) results only from wing twist. From Eq. (17), this second term can be related to the basic lift contribution to root bending moment coefficient for the wing. Thus, using the definition in Eq. (23), Eq. (42) can be written as

$$
C_{m_{ac}} \;=\; \frac{\bar{c}_{mac}}{c_{\text{ref}}} \overline{\overline{\widetilde{C}}}_{m_{ac}} - \frac{2 \tan \Lambda}{c_{\text{ref}}/b} (C_{\ell_{b0}})_{\text{left}}
\tag{43}
$$

where

$$
(C_{\ell_{b0}})_{\text{left}} \;\equiv\; \frac{1}{Sb} \int_{z=0}^{b/2} \widetilde{C}_{L_b} \, c \, z \, dz
\tag{44}
$$

From Eq. (27), we see that the term defined in Eq. (44) is equal to the twist contribution to the root bending moment coefficient.

For wings with no sweep or dihedral, the integral on the right-hand side of Eq. (44) was previously evaluated from Eq. (15) to give the second term on the right-hand side of Eq. (28). Using the approximation of Anderson [22] that was used to obtain Eq. (32), a first approximation to Eq. (44) for swept wings could be taken as

$$(C_{\ell_{b0}})_{\text{left}} \cong -\kappa_{M\Omega} \frac{C_{L,\alpha}\,\Omega}{2} \qquad (45)$$

where $\kappa_{M\Omega}$ is defined by Eq. (29). Thus, a first approximation for the pitching moment produced about the aerodynamic center of a swept wing could be obtained by using Eq. (45) in Eq. (43), which yields

$$C_{m_{ac}} \cong \frac{\bar{c}_{mac}}{c_{\text{ref}}} \widetilde{\overline{C}}_{m_{ac}} + \kappa_{M\Omega} \frac{\tan \Lambda}{c_{\text{ref}}/b} C_{L,\alpha}\,\Omega \qquad (46)$$

Improved results are obtained from Eq. (46) if the actual lift slope for the swept wing is used in this relation. Thus, to obtain best results from Eq. (46) we require some means for estimating the lift slope for the swept wing.

From Eq. (14), the lift slope for an unswept wing can be written as $C_{L,\alpha} = \pi R_A a_1$. This suggests that the lift slope for a swept wing could be expressed as

$$C_{L,\alpha} = \pi R_A a_1 \kappa_{L\Lambda} \qquad (47)$$

where $\kappa_{L\Lambda}$ is an empirical sweep correction factor and $a_1$ is evaluated from Eq. (11) for an unswept wing having the same taper and aspect ratio. Figure 13 shows a correlation for $\kappa_{L\Lambda}$ as a function of sweep, taper, and aspect ratio, which was obtained from the results of the present CFD study. This correlation was obtained using only the results for untwisted wings having the NACA 0012 airfoil section. Figure 14 shows all CFD results obtained in the present study compared with results predicted from Eq. (47) using the values for $\kappa_{L\Lambda}$ that are plotted in Fig. 13.

A comparison between pitching moment results predicted from Eq. (46) and the CFD results obtained in the present study is shown in Fig. 15. Because only wings with twist and/or camber produce a pitching moment about the aerodynamic center of the wing, all of the results for untwisted wings without camber fall in the tightly grouped cluster of points at the origin of Fig. 15. Notice that the magnitude of the pitching moment about the aerodynamic center is always slightly less than that predicted from Eq. (46). This suggests an empirical correction to Eq. (46) of the form

$$C_{m_{ac}} \cong \frac{\bar{c}_{mac}}{c_{\text{ref}}} \widetilde{\overline{C}}_{m_{ac}} + \kappa_{M\Omega} \frac{\tan(\kappa_{M\Lambda}\,\Lambda)}{c_{\text{ref}}/b} C_{L,\alpha}\,\Omega \qquad (48)$$

where $\kappa_{M\Lambda}$ is a sweep correction factor. Figure 16 shows a correlation for $\kappa_{M\Lambda}$ as a function of taper and aspect ratio, which was obtained from the results of the present CFD study. This correlation was obtained using only the results for twisted wings having the NACA 0012 airfoil section. Figure 17 shows all CFD results obtained in the present study compared with results predicted from Eq. (48) using the values for $\kappa_{M\Lambda}$ that are plotted in Fig. 16.
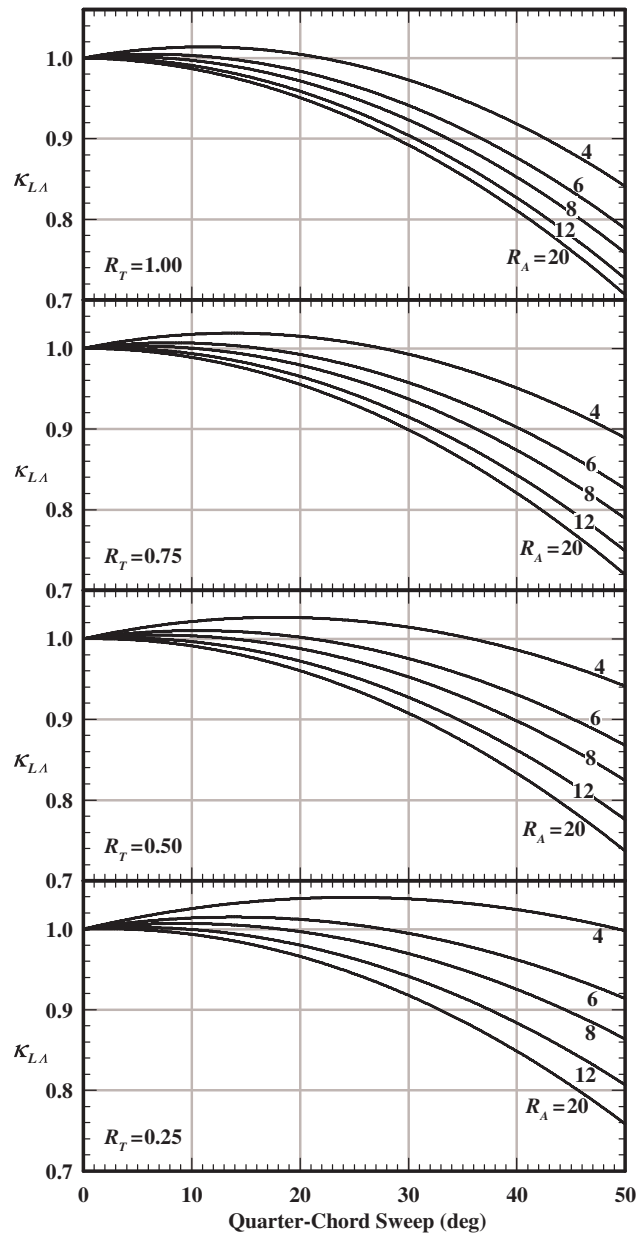


**Fig. 13 Effects of wing sweep on the lift slope.**
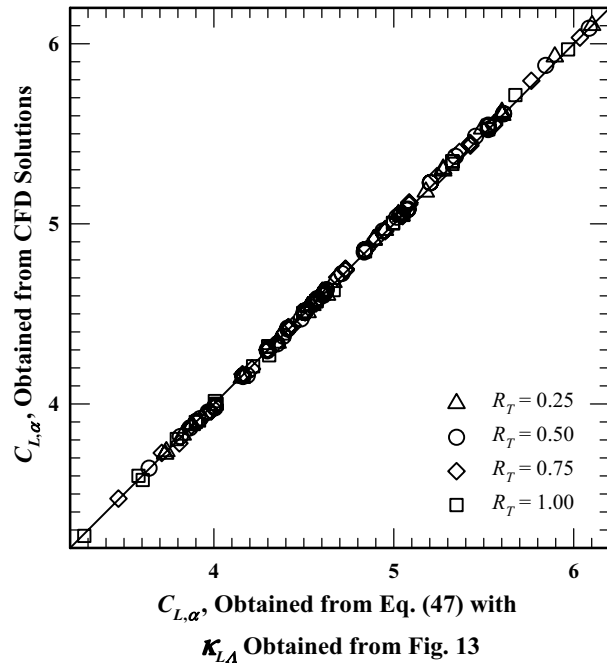
**Fig. 14   Lift slope as predicted from CFD results compared with predictions from Eq. (47) and Fig. 13.**
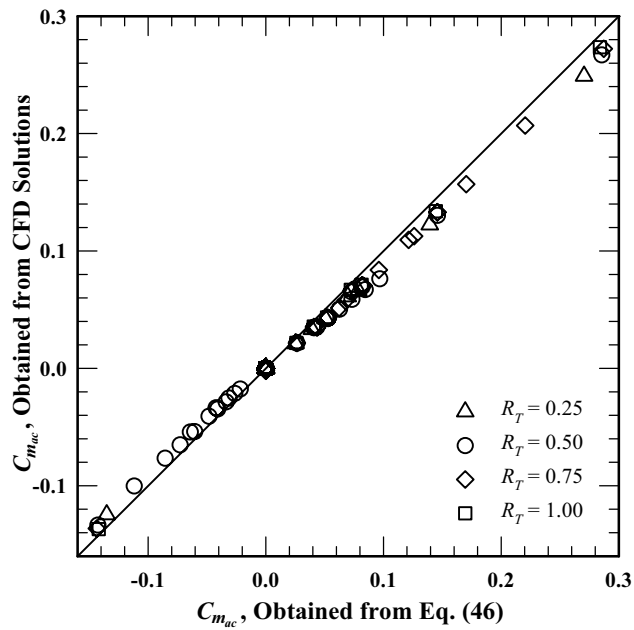


**Fig. 15   Pitching moment coefficients predicted from CFD results compared with predictions from Eq. (46).**
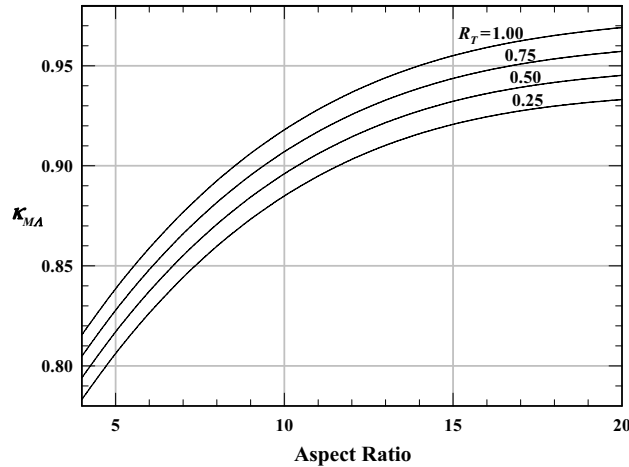
**Fig. 16  Sweep factor in the relation for wing pitching moment about the wing aerodynamic center.**
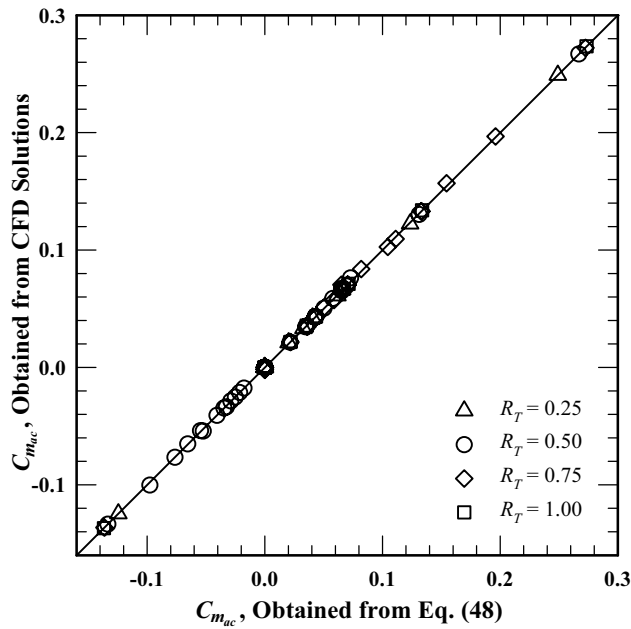


**Fig. 17  Pitching moment coefficients predicted from CFD results compared with predictions from Eq. (48).**

Equation (48) reveals the effectiveness of twisted, swept wings for balancing the pitching moment on a stable airplane.  The first term is typically negative due to positively cambered wings.  The second term is positive for positive washout and positive sweep.  Consequently, positive twist on a swept-back wing can be used to create the positive zero-lift pitching moment required for balanced flight in a stable airplane, particularly those without a horizontal stabilizer.

## Conclusions

Results presented here allow one to obtain improved estimates for the location of the aerodynamic center of wings with constant linear taper and constant quarter-chord sweep. For unswept wings with linear taper, the spanwise coordinate of the semispan aerodynamic center can be obtained from Eq. (25) or Fig. 5. These results can be adjusted to estimate the axial coordinate of the aerodynamic center of swept wings by applying Eq. (36). The sweep factor in Eq. (36) can be obtained from Fig. 11. For the wing geometries considered in the present study, the position of the wing aerodynamic center depends only on aspect ratio, taper ratio, and the quarter-chord sweep angle. Within the range of parameters studied, wing camber, thickness, and twist were shown to have no significant effect on the position of the wing aerodynamic center.

Results are also present that allow one to obtain improved estimates for the moment components produced by wings with constant linear taper and constant quarter-chord sweep. For unswept wings, the root wing bending moment can be estimated from Eq. (28). The twist factor in Eq. (28) can be obtained from Eq. (29), or for the case of wings with linear taper and linear washout, Fig. 6 can be used. For wings with constant sweep, the pitching moment about the aerodynamic center can be estimated from Eq. (48). The lift slope in Eq. (48) is that for the swept wing, which can be estimated from Eq. (47) using the sweep factor obtained from Fig. 13. The twist factor used in Eq. (48) is that for an unswept wing, which is obtained from Eq. (29). The sweep factor in Eq. (48) is obtained from Fig. 16. Within the range parameters studied, Eq. (48) agrees closely with the CFD results.

## Acknowledgement

## References

[1]   Etkin, B., and Reid, L. D., "Mean Aerodynamic Chord, Mean Aerodynamic Center, and $C_{m_{ac}}$," *Dynamics of Flight: Stability and Control*, 3rd ed., Wiley, New York, NY, 1996, pp. 357–363.

[2]    McCormick, B. W., "Aerodynamic Center Location for a Finite Wing, $C_{m_{ac}}$, and Mean Aerodynamic Chord (MAC)" *Aerodynamics, Aeronautics, and Flight Mechanics*, 2nd ed. Wiley, New York, 1995, pp. 126–128.

[3]    Pamadi, B. N., "Wing Planform Parameters" and "Concept of Aerodynamic Center," *Performance, Stability, Dynamics, and Control of Airplanes*, 2nd ed., AIAA, Reston, VA, 2004, pp. 15–17 and 20–22.

[4]    Raymer, D. P., "Wing Geometry," *Aircraft Design: A Conceptual Approach*, 2nd ed., AIAA, Washington, DC, 1992, pp. 47–65.

[5]    Prandtl, L., "Tragflügel Theorie," *Nachricten von der Gesellschaften zu Göttingen*, Geschäeftliche Mitteilungen, Klasse, Germany, 1918, pp. 451–477.

[6]    Prandtl, L., "Applications of Modern Hydrodynamics to Aeronautics," NACA TR-116, June 1921.

[7]    Glauert, H., "The Monoplane Aerofoil," *The Elements of Aerofoil and Airscrew Theory*, Cambridge University Press, Cambridge, UK, 1926, pp. 137–155.

[8]    Multhopp, H., "Die Berechnung der Auftriebs Verteilung von Tragflugeln," *Luftfahrtforschung*, Vol. 15, No. 14, 1938, pp. 153–169.

[9]    Lotz, I., "Berechnung der Auftriebsverteilung beliebig geformter Flugel," *Zeitschrift für Flugtechnik und Motorluftschiffahrt*, Vol. 22, No. 7, 1931, pp. 189–195.

[10]   Karamcheti, K., "Elements of Finite Wing Theory," *Ideal-Fluid Aerodynamics*, Wiley, New York, 1966, pp. 535–567.

[11]   Anderson, J. D., "Incompressible Flow over Finite Wings: Prandtl's Classical Lifting-Line Theory," *Fundamentals of Aerodynamics*, 3rd ed., McGraw-Hill, New York, 2001, pp. 360–387.

[12]   Bertin, J. J., "Incompressible Flow About Wings of Finite Span," *Aerodynamics for Engineers*, 4th ed., Prentice-Hall, Upper Saddle River, New Jersey, 2002, pp. 230–302.

[13]   Katz, J., and Plotkin, A., "Finite Wing: The Lifting-Line Model," *Low-speed Aerodynamics*, 2nd ed., Cambridge University Press, Cambridge, UK, 2001, pp. 167–183.

[14]   Kuethe, A. M., and Chow, C. Y., "The Finite Wing," *Foundations of Aerodynamics*, 5th ed., Wiley, New York, 1998, pp. 169–219.

[15]   McCormick, B. W., "The Lifting-Line Model," *Aerodynamics, Aeronautics, and Flight Mechanics*, 2nd ed. Wiley, New York, 1995, pp. 112–119.

[16] Phillips, W. F., "Incompressible Flow over Finite Wings," *Mechanics of Flight*, Wiley, Hoboken, NJ, 2004, pp. 42–79.

[17] Phillips, W. F., "Lifting-Line Analysis for Twisted Wings and Washout-Optimized Wings," *Journal of Aircraft*, Vol. 41, No. 1, 2004, pp. 128–136.

[18] Phillips, W. F., Alley, N. R., and Goodrich, W. D., "Lifting-Line Analysis of Roll Control and Variable Twist," *Journal of Aircraft*, Vol. 41, No. 5, 2004, pp. 1169–1176.

[19] Phillips, W. F., Fugal, S. R., and Spall, R. E., "Minimizing Induced Drag with Wing Twist, Computational-Fluid-Dynamics Validation," *Journal of Aircraft*, Vol. 43, No. 2, 2006, pp. 437–444.

[20] Phillips, W. F., and Alley, N. R., "Predicting Maximum Lift Coefficient for Twisted Wings Using Lifting-Line Theory," *Journal of Aircraft*, accepted for publication, Sept. 2006.

[21] Anderson, R. F., "Charts for Determining the Pitching Moment of Tapered Wings with Sweepback and Twist," NACA TN-483, Dec. 1933.

[22] Anderson, R. F., "Determination of the Characteristics of Tapered Wings," NACA TR-572, Feb. 1937.

[23] Kolbe, C. D., and Boltz, F.W., "The Forces and Pressure Distribution at Subsonic Speeds on a Plane Wing Having 45° of Sweepback, Aspect Ratio of 3, and a Taper Ratio of 0.5," NACA RM-A51G31, Oct. 1951.

[24] Graham, R. R., "Low-Speed Characteristics of a 45° Sweptback Wing of Aspect Ratio 8 from Pressure Distributions and Force Tests at Reynolds Numbers from 1,500,000 to 4,800,000," NACA RM-L51H13, Oct. 1951.

[25] Weber, J., and Brebner, G. G., "Low-Speed Tests on 45-deg Swept-Back Wings, Part I: Pressure Measurements on Wings of Aspect Ratio 5," RM-2882, Aeronautical Research Council, London, May 1958.

[26] Hall, I. M. and Rogers, E. W. E., "Experiments with a Tapered Sweptback Wing of Warren 12 Planform at Mach Numbers Between 0.6 and 1.6," RM-3271, Aeronautical Research Council, London, June 1962.

[27] Kuchemann, D., "A Simple Method for Calculating the Span and Chordwise Loading on Straight and Swept Wings of any Given Aspect Ratio at Subsonic Speeds," RM-2935, Aeronautical Research Council, London, May 1956.

[28] Krist, S.L., Biedron, R.T., and Rumsey, C.L., "CFL3D Users Manual (Version 5)", NASA TM-1998-208444, June 1998.

[29] Roe, P.L., "Approximate Reimann Solvers, Parameter Vectors, and Difference Schemes," *Journal of Computational Physics*, Vol. 43, Feb., 1981, pp. 357–372.

[30] Richardson, L.F., "The Approximate Arithmetical Solution by Finite Differences of Physical Problems Involving Differential Equations, with an Application to the Stresses In a Masonry Dam," *Transactions of the Royal Society of London, A*, Vol. 210, Jan., 1910, pp. 307–357.

[31] Richardson L.F. and Gaunt, J. A., "The Deferred Approach to the Limit," *Transactions of the Royal Society of London, A*, Vol. 226, Jan., 1927, pp. 299–361.